



Phase-field simulation of the spinodal decomposition process near moving grain boundaries

Can Guo^{a,*}, Ying Gao^a, Yu-teng Cui^a, Yu-ping Zhao^b, Chun-jie Xu^{a,*}, Shang Sui^a, Xiang-quan Wu^a, Zhong-ming Zhang^a

^a School of Materials Science and Engineering, Xi'an University of Technology, Xi'an 710048, China

^b School of Materials Science and Engineering, Hebei University of Technology, Tianjin 300401, China



ARTICLE INFO

Keywords:
Spinodal decomposition
Grain boundary migration
Pattern formation
Phase-field simulation

ABSTRACT

Many investigations show that the grain boundary can significantly affect the pattern formation and kinetics of spinodal decomposition, however, these works rarely consider the effects of the kinetic properties of grain boundaries. In this work, the spinodal decomposition process near moving grain boundaries was investigated by the phase-field model. The simulation results indicate that the grain boundary-directed spinodal pattern is anisotropic, and with the increase of atom mobility inside the grain boundary, the pattern of the decomposed phase changes from parallel to the original grain boundary to perpendicularity. Moreover, the spinodal decomposition also affects the migration process of the grain boundary in turn.

1. Introduction

It is well known that the grain boundary plays a key role in solid phase transformations, which mainly due to the loose atomic structures and high chemical potential make it a perfect place for element segregation and the formation of new phases [1,2]. Recent investigations have shown that the grain boundary can significantly affect the kinetics of spinodal decomposition [3–7]. Li, Rajeshwari, and Grönhagen et al. [4,6,8] reported that spinodal decomposition often starts earlier near defects or grain boundaries. Moreover, the pattern formation of spinodal decomposition is affected by the properties of the grain boundaries. For example, Liu et al. [9] reported that the decomposed phases are alternating layers parallel to the grain boundary. While the results of Li et al. [6,10,11] show that the pattern of the decomposed phases is perpendicular to the grain boundary. Deng et al. [7] calculated the energy state of grain boundary-directed spinodal decomposition and indicated that the pattern selection might be controlled by the grain boundary energy and the concentration gradient energy.

Previous investigations show us some new insights about grain boundary directed spinodal decomposition, however, these studies rarely take the influence of grain boundary kinetic properties on the spinodal decomposition processes into consideration. For example, for nanocrystalline materials, the migration of grain boundary is very common [12,13], now the grain boundary-directed spinodal pattern

would be very different [14,15]. As spinodal decomposition is usually too fast to be captured in experiments, the pattern formation mechanism and the interaction process of moving grain boundaries and spinodal decomposition remain unclear. Fortunately, with the rapid development of computer technologies, numerical methods have become powerful tools to study microstructure evolution processes with multi-physical fields [16–19]. Among these, the phase-field model is widely used to model spinodal decomposition and the evolution of complex phase boundaries [20–26].

In this work, the phase-field model built by Ramanarayanan et al. [27] was used to investigate the spinodal decomposition process near moving grain boundaries. We simulated the microstructure evolution of two-grain systems with different initial average compositions and discussed the influence of moving grain boundaries on the selection of spinodal patterns. The simulation results could expand our knowledge of spinodal decomposition with the existence of moving grain boundaries.

2. Phase-field model

The total free energy of the binary phase-field model is written as [27],

$$F = \int dV \left\{ f(c, \eta_i) + k_c (\nabla c)^2 + \sum_i k_\eta (\nabla \eta_i)^2 \right\} \quad (1)$$

* Corresponding authors.

E-mail addresses: cguo@xaut.edu.cn (C. Guo), xuchunjie@xaut.edu.cn (C.-j. Xu).

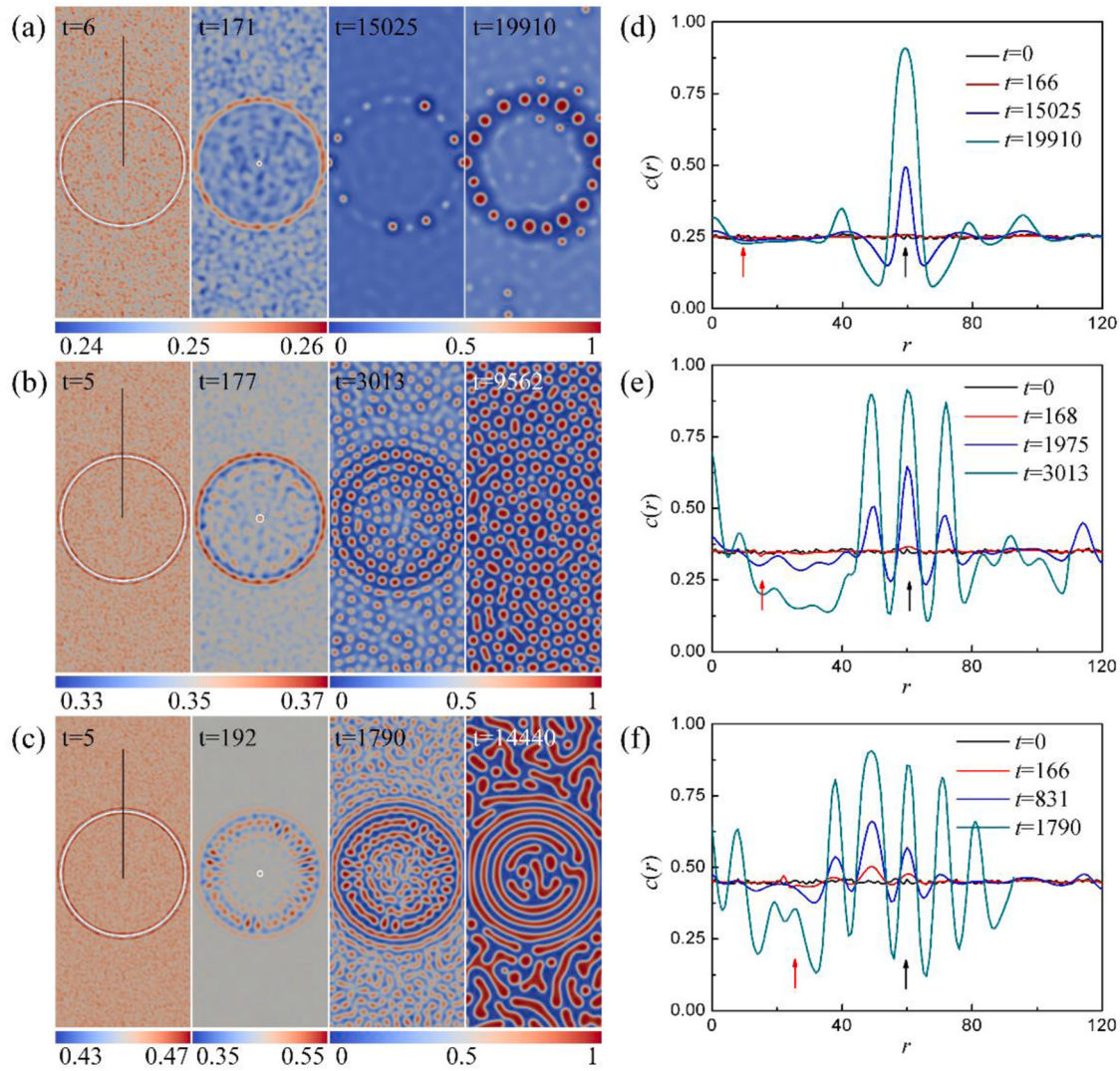


Fig. 1. a-c are the snapshots of the spinodal decomposition process with different initial average compositions c_0 with $M_t = 500$, where (a) $c_0 = 0.25$, (b) $c_0 = 0.35$, (c) $c_0 = 0.45$, and the solid white line is the grain boundary; d-f are the temporal evolution of the concentration field along the solid black line in a-c, where the arrows point to the positions of the grain boundary.

where c is the concentration field, η_i is an order parameter field describing the grain i , $f(c, \eta_i)$ is the bulk free energy density, the second term and third term represent the concentration gradient energy and grain boundary energy [28], respectively. Here, $f(c, \eta_i)$ is [27],

$$f(c, \eta_i) = Ac^2(1 - c)^2 + m(c) \left[0.25 + \sum_i \left(\frac{\eta_i^4}{4} - \frac{\eta_i^2}{2} \right) + \varepsilon \sum_i \sum_{j>i} \eta_i^2 \eta_j^2 \right] \quad (2)$$

where A and ε are constants, $m(c)$ is a function that couples the concentration field with the order parameter field, and the formula of $m(c)$ affects the solute segregation in the grain boundary [29], herein, $m(c) = 1 + 0.5c^2 - 0.25c^2(1 - c)^2$.

The evolution equation of the concentration field c is,

$$\frac{\partial c(r, t)}{\partial t} = \nabla \left(M_c \nabla \frac{\partial F}{\partial c} \right) + \xi_c \quad (3)$$

where ξ_c is Langevin Noise, the weak form of the noise term is $(2\chi - 1)\alpha P(\vec{r})c$, where χ is a random number in $[0 \dots 1]$, the amplitude α is 0.01 , $P(\vec{r})$ is a location position dependent function. M_c is a constant [27],

$$M_c = M_b + \varphi_g M_t \quad (4)$$

where M_b and M_t are atomic mobility constants for the bulk region and the grain boundary, respectively, and $\varphi_g = [\sum_i \sum_{j>i} \eta_i^2 \eta_j^2]^{1/2}$.

The evolution equation of η_i is,

$$\frac{\partial \eta_i(r, t)}{\partial t} = -L \frac{\partial F}{\partial \eta_i} | i = 1, 2, 3 \dots n \quad (5)$$

where $L = 1$ is a constant relaxation coefficient. The Eq. 4 and Eq. 5 were solved by the open-source Multiphysics Object-Oriented Simulation Environment (MOOSE) [30]. The size of simulation box for 2D is $L_x \times L_y = 400 \Delta x \times 128 \Delta y$, and it is $L_x \times L_y \times L_z = 80 \Delta x \times 80 \Delta y \times 80 \Delta z$ for 3D. All the simulations are performed with periodic boundary conditions, and adaptive time step method, where $\Delta x = \Delta y = 1$.

3. Results and discussion

Figs. 1a-1c show the snapshots of the concentration field evolution process with different initial average compositions c_0 , where $c_0 = 0.25$ (Fig. 1a), $c_0 = 0.35$ (Fig. 1b), and $c_0 = 0.45$ (Fig. 1c), the solid white line

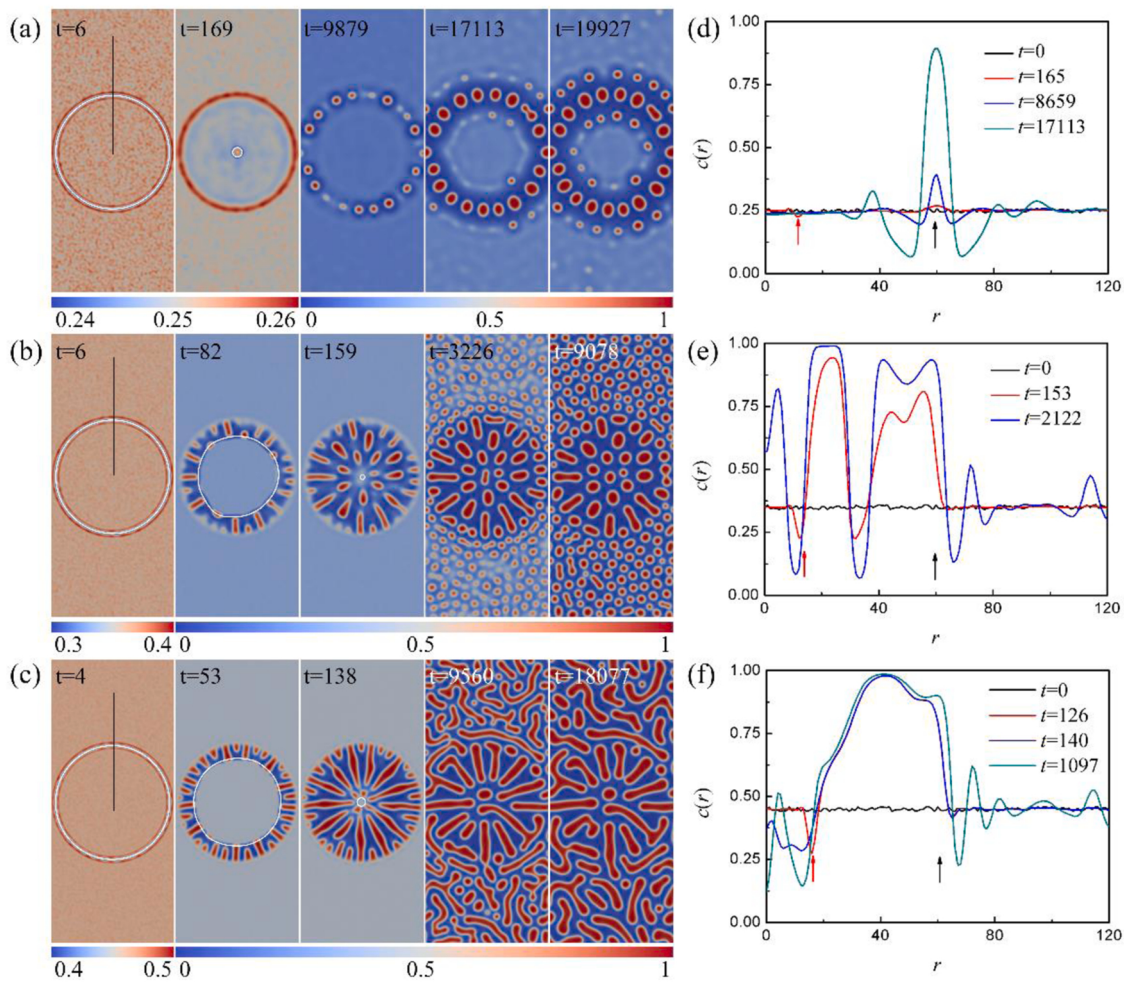


Fig. 2. a-c are the snapshots of the spinodal decomposition process with different c_0 with $M_t = 1000$, where $c_0 = 0.25, 0.35$, and 0.45 ; d-f are the temporal evolution of the concentration field along the solid black line in a-c.

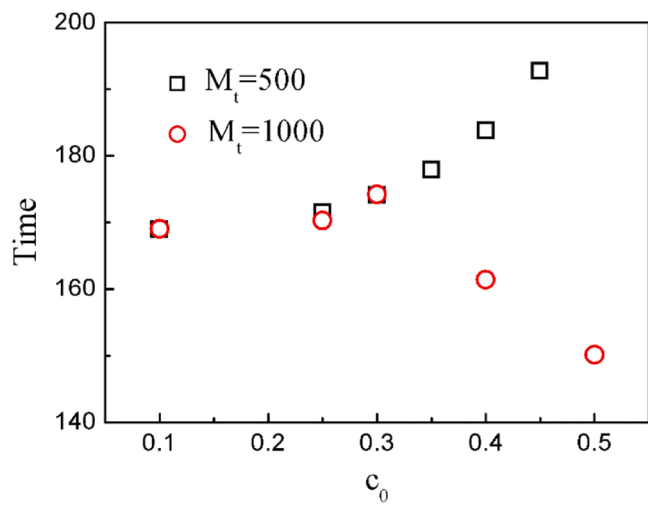


Fig. 3. The migration time of the moving grain boundaries with different M_t and c_0 .

is the grain boundary, the initial curvature radius of the grain boundary is $60\Delta x$, the concentration gradient parameter $kc = 1$, the grain boundary energy parameter $k\eta = 1$, the phase decomposition is induced by random noise. Figs. 1d-1f show the concentration field along the solid

black line in Figs. 1a-1c, where the arrows point to the positions of the grain boundary. The atomic mobility constants in Eq. 4 are $M_b = 1$ and $M_t = 500$. It can be seen that, during the evolution process, the curvature-driven grain boundary migration process and the spinodal decomposition process happen simultaneously, and the phase decomposition always begins at the initial location of the grain boundary which is consistent with the previous results [7,29]. As the selection segregation of the alpha phase at the grain boundaries, the amplitude of the concentration field is larger for the region where the grain boundary once passed, as shown in Figs. 1d-1f. The moving grain boundary leaves behind a series of alternate domains of the two decomposed phases, thus the spinodal decomposition velocity is faster in the central grain. Comparing the concentration evolution with different initial c_0 , the spinodal decomposition velocity and the influence of the grain boundary increase in c_0 . For $c_0 = 0.25$, the volume fraction of the beta phase is very limited, and the beta-phase particles only distribute near the position of the initial grain boundary in a ring pattern, as shown in Fig. 1a and Fig. 1d at $t = 19,910$. When c_0 increases to 0.35, the beta-phase particles inside the internal grain distribute in concentric rings parallel to the grain boundary, while it distributes randomly in the external grain. As for $c_0 = 0.45$, the granular beta-phase transformed into a striped one, and the spinodal pattern is an alternating alpha and beta layers that parallel to the grain boundary in the internal grain and isotropic continuous microstructures in other regions. These results indicate that although the grain boundary migration velocity is far more quickly than the phase decomposition process, the grain boundary-induced phase segregation behavior still affects the kinetics

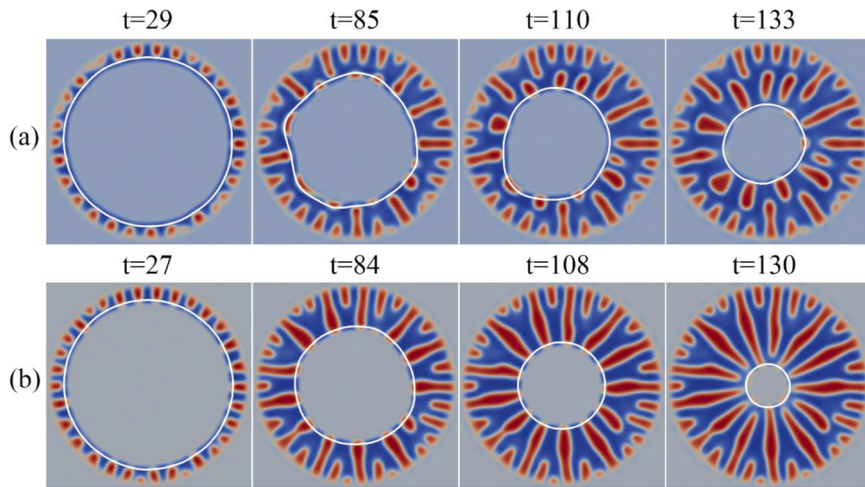


Fig. 4. The concentration field evolution process with different c_0 with $M_t = 1000$, where $c_0 = 0.4$ (Fig. 4a) and 0.5 (Fig. 4b), the solid white line is the grain boundary.

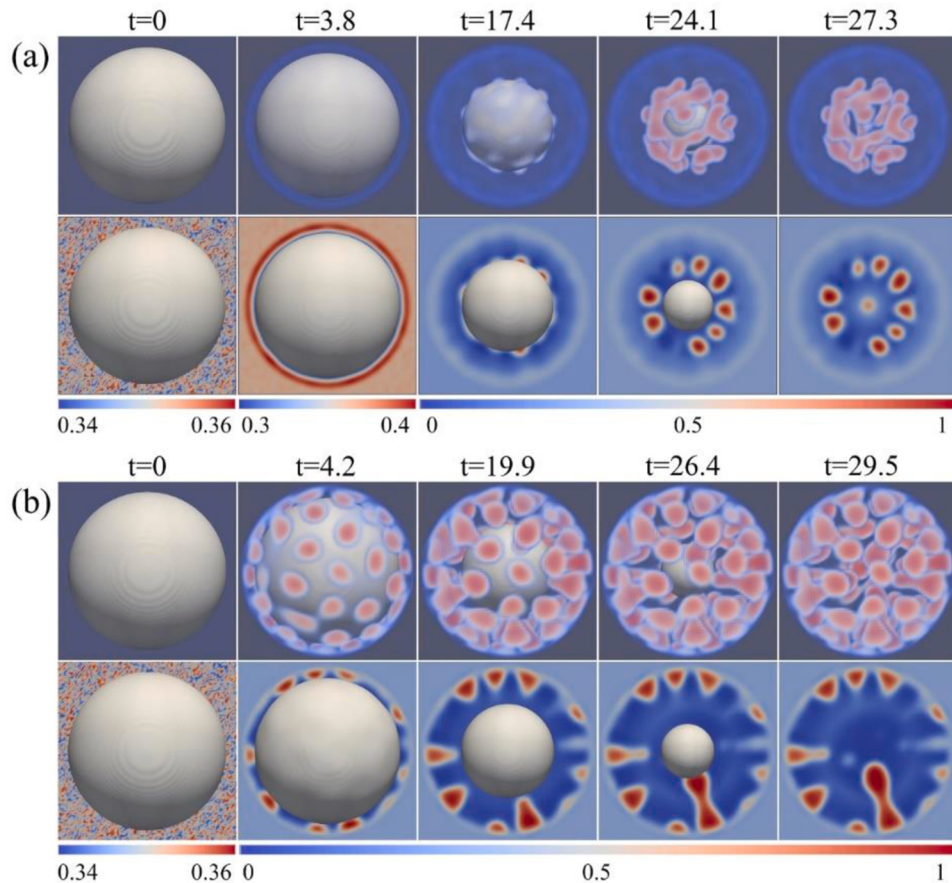


Fig. 5. The concentration field evolution process with different M_t for $c_0 = 0.35$, where $M_t = 1000$ (Fig. 5 a), and $M_t = 5000$ (Fig. 5 b), the snapshots in the first row are 3D views, the snapshots in the second row are 2D sectional views at the position of $L_x = 40\Delta x$, the solid white spherical surface is the grain boundary with initial radius equal to $35\Delta x$.

and the morphology of spinodal decomposition.

Further, we simulated the spinodal decomposition near moving grain boundaries with higher atom mobility constant (where $M_t = 1000$), as shown in Fig. 2, Figs. 2a-2c are the snapshots of the spinodal decomposition process with $c_0 = 0.25, 0.35$, and 0.45, and Figs. 2d-2f are the temporal evolution of the concentration fields along the solid black line in Figs. 2a-2c. One can see that, for $c_0 = 0.25$ as shown in Fig. 2a, due to

the driving force for phase decomposition being weak, the spinodal decomposition velocity is still very slow, and the interaction between the phase decomposition and the grain boundary is weak, the evolution process and the final microstructure pattern are similar to the result in Fig. 1a. For c_0 larger than 0.35, different with the results in Fig. 1, the spinodal decomposition was done in two stages, central grain phase transition or grain boundary-directed spinodal decomposition process

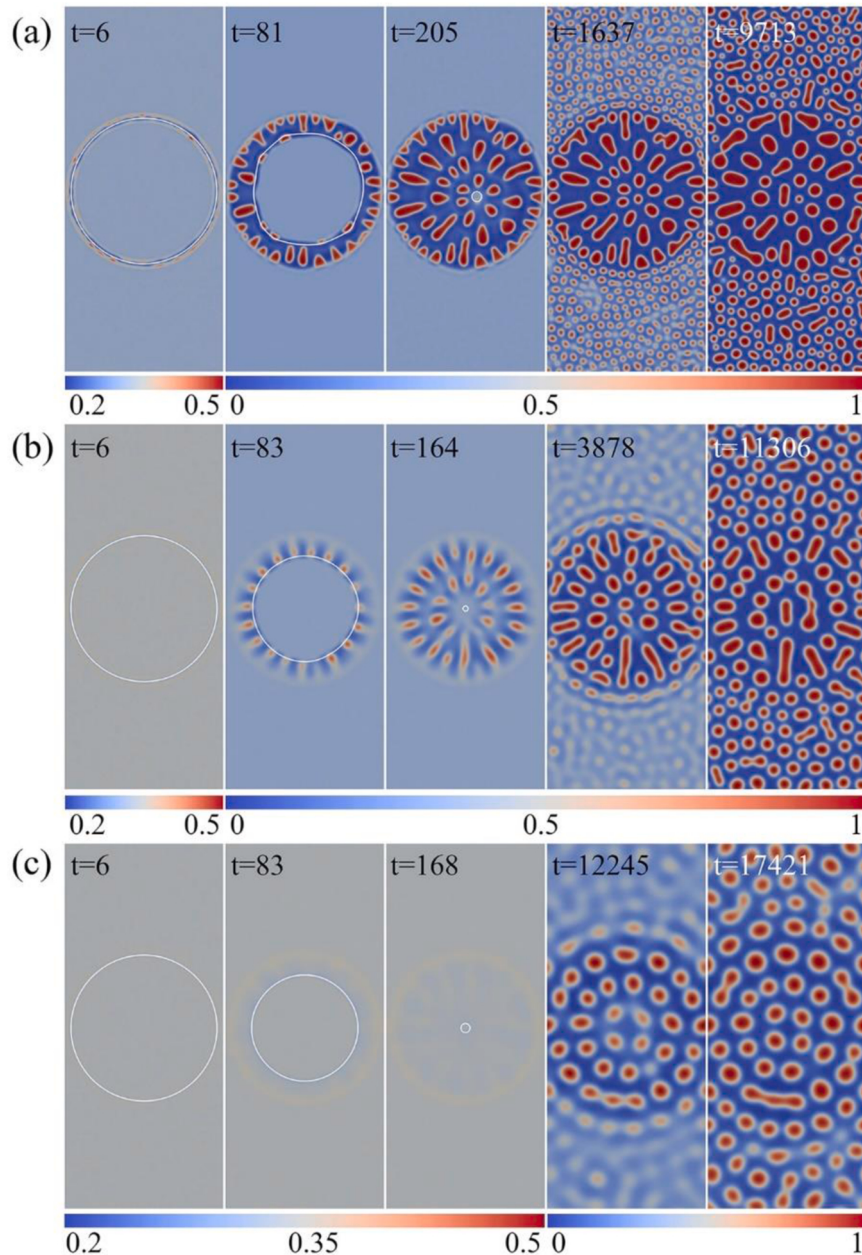


Fig. 6. The snapshots of the spinodal decomposition process with different concentration gradient energy parameters kc when $M_t = 1000$, where (a) $kc = 0.5$, (b) $kc = 1.5$, (c) $kc = 2.0$, and the solid white line is the grain boundary.

(Stage I) and external grain phase transition or bulk spinodal decomposition process (Stage II). In Stage I, the concentration waves start at the position of the initial grain boundary, then extend to the center of the internal grain as shown in Fig. 2b and Fig. 2c. Due to the increased atom mobility constant near the grain boundaries, the amplitude of the concentration fields reach the equilibrium value very quickly as shown in Fig. 2e and Fig. 2f. During this stage, the frontier of the phase decomposition always accompanying with the moving grain boundary, and the phase transition process is finished when the grain boundary moving out of the simulation region. Finally, obtaining microstructure perpendicular to the original grain boundary, the beta phase is short rod-shaped for $c_0 = 0.35$ and is striped for $c_0 = 0.45$. And then, after a long time of relaxation, it enters the second stage phase transition and obtains particle-shaped beta phase for $c_0 = 0.35$ and isotropic continuous microstructures for $c_0 = 0.45$, which is similar to the results in Fig. 1.

From the results in Fig. 1 and Fig. 2, the moving grain boundary affects the evolution kinetics and pattern formation of spinodal

decomposition, at the same time the phase decomposition also affects the migration process of the grain boundaries. Fig. 3 shows the migration time of the grain boundary with different M_t and c_0 . For $M_t = 500$, the time required for grain boundary migration increases with the c_0 . This is due to the amplitude of the grain boundary segregation-induced concentration wave in the front of the grain boundary increasing with c_0 , as shown in Figs. 1d-1f, which opposed the migration of the grain boundary. As for $M_t = 1000$, the migration time increases first and then decreases with the increase in c_0 . This is because the phase decomposition driving force is very small when c_0 is less than 0.3, the interaction between the spinodal decomposition and the moving grain boundary is relatively weak, and the microstructure evolution processes for $M_t = 500$ and 1000 are similar. To c_0 larger than 0.35, the phase decomposition is easier [31], now the frontier of the phase decomposition always accompanies the moving grain boundary, and the excluded solutes by the grain boundary will attach to the existing beta phase directly. Then the pinning effects of solute atoms on the migration of grain

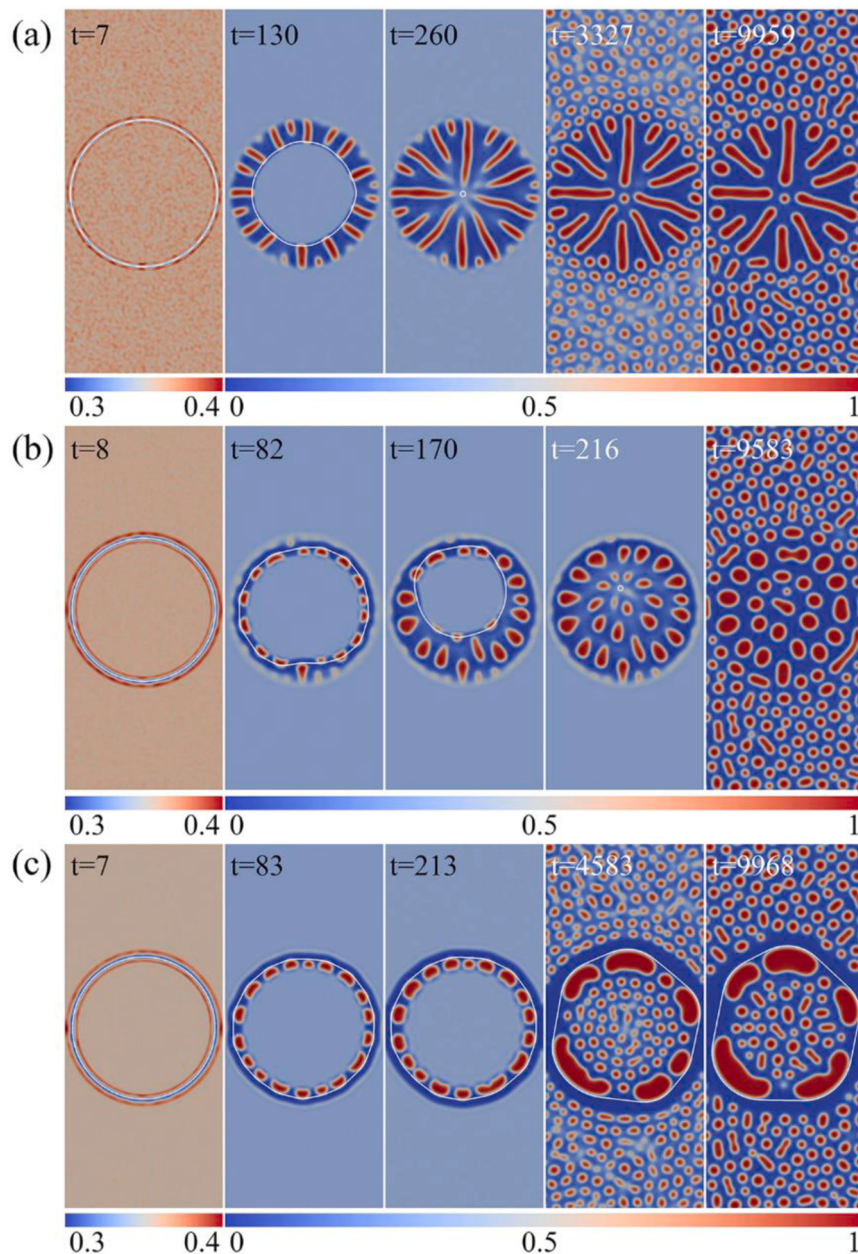


Fig. 7. The snapshots of the spinodal decomposition process with different grain boundary energy parameters $k\eta$ when $M_t = 1000$, where (a) $k\eta = 0.5$, (b) $k\eta = 1.5$, and (c) $k\eta = 2.0$, and the solid white line is the grain boundary.

boundaries become weaker, and the migration time is shortened.

For better understanding of the interaction process between the spinodal decomposition and the moving grain boundaries, Fig. 4 shows the concentration field evolution process with different c_0 with $M_t = 1000$, where $c_0 = 0.4$ (Fig. 4a) and 0.5 (Fig. 4b). As shown in Fig. 4a at $t = 85$, the excluded solute atoms aggregate on both sides of the grain boundary simultaneously, and the solutes located in the path of grain boundary migration would pin the grain boundaries. Until the local curvature becomes large enough to overcome the pinning force from the beta phase domains, the grain boundary continues to migrate. Once the grain boundary crossed the beta domains, the excluding solute atoms will attach to these newly formed beta domains immediately and will no longer impede the migration of the grain boundary. When c_0 increases to 0.5, the volume fraction of the beta phase becomes larger, and the shape of the beta phase changes from short rods to long strips. Now, the moving grain boundary is always the frontier of spinodal decomposition, the solute atoms will not aggregate in the front of grain boundary as

shown in Fig. 4b, and the phase decomposition no longer pinning the grain boundary, which leads to the decrease of migration time as shown in Fig. 3.

Fig. 5 shows the concentration field evolution process with different M_t in three-dimension for $c_0 = 0.35$, where $M_t = 1000$ (Fig. 5a), and $M_t = 5000$ (Fig. 5b), the snapshots in the first row are 3D views, the snapshots in the second row are 2D sectional views at the position of $L_x = 40\Delta x$, the solid white spherical surface is the grain boundary with initial curvature radius equal to $35\Delta x$. It is clear that the phase decomposition inside the interior grain is much easier under the influence of the grain boundary, and the phase transition velocity increases with the M_t . For $M_t = 1000$, the pattern of beta-phase is concentric rings parallel to the initial grain boundary in 2D sectional view which is same with the results in Fig. 1b, however, most of the beta-phase domains are connected in the third dimension and it is an isotropic continuous microstructure actually. When M_t increases to 5000, the frontier of the phase decomposition accompanies the moving grain boundary and

forms a spinodal pattern with anisotropy. Now, the distribution of beta-phase becomes more dispersed, and it is liquid-drop or short-rod shaped along the direction perpendicular to the original grain boundary, this is consistent with the results in Fig. 2b. Compared with the results in Fig. 1 and Fig. 2, although the morphology of the decomposed phases is more complex in 3D, the influence mechanisms of moving grain boundary on the spinodal decomposition remain unchanged.

From the results above, the pattern formation of grain boundary-directed spinodal decomposition is significantly affected by the phase decomposition velocity and migration of the grain boundary. Further, we simulated the spinodal decomposition process with different gradient term parameters k_c and k_η , as shown in Fig. 6 and Fig. 7, respectively. The concentration gradient energy is proportional to $\sqrt{k_c}$ and the grain boundary energy is proportional to $\sqrt{k_\eta}$ [28]. As the resistance of phase decomposition increases with the concentration gradient energy, the spinodal decomposition velocity decreases with k_c , and the microstructure of decomposed phases becomes more coarsen for larger k_c as shown in Fig. 6. For $k_c = 0.5$, the amplitude of the concentration waves reaches the maximum value very fast, now the grain boundary is always the frontier of phase decomposition and forms patterns perpendicular to the grain boundary. With the increase of k_c , the increase of wave amplitudes becomes slow, when $k_c = 2$, the velocity of phase decomposition is very slow and the influence of the moving grain boundary on the spinodal decomposition becomes very weak and forms a concentric ring pattern finally.

Fig. 7 shows the spinodal decomposition process with different grain boundary energy parameters k_η when $M_t = 1000$, where $k_\eta = 0.5$ (Fig. 7a), $k_\eta = 1.5$ (Fig. 7b), $k_\eta = 2.0$ (Fig. 7c). For $k_\eta = 0.5$, the two decomposed phases are alternating layers perpendicular to the grain boundary, due to the length of the grain boundary decreases with time, the growth of some of the beta-phase layers are terminated. With the increase of grain boundary energy, the volume fraction of decomposed beta phases that are parallel to the grain boundary increases gradually, and the morphology of the grain boundary modulated beta phase shifts from layer-shaped (Fig. 7a) to short rod-shaped (Fig. 2b, where $k_\eta = 1.0$) to liquid drop shaped (Fig. 7b) and then flake shaped (Fig. 7c). Deng et al. [7] calculated the local energy of grain boundary directed spinodal decomposition, they reported that, for high grain boundary energy conditions, the decomposed phases are parallel to the grain boundary, this is consistent with our simulation results. Further, we checked the migration time (t) of the grain boundaries, where $t = 210$ (Fig. 7a), 159 (Fig. 2b), 216 (Fig. 7b), and larger than 9968 (Fig. 7c), as the increase of k_η the migration time decreases first and then increases rapidly. The increase of t is caused by the pinning of beta domains ahead of the grain boundary. As the volume fraction and the size of the beta phase near the grain boundary increase with k_η , the migration of grain boundary will be more difficult for high energy grain boundaries, which then causes a rapid increase in migration time.

4. Conclusion

In conclusion, the spinodal decomposition process near moving grain boundaries was investigated by the phase-field model. Similar to the previous numerical and experimental results [6,10,32], our simulations also show that the grain boundary could stimulate the spinodal decomposition process. The grain boundary-directed spinodal pattern is anisotropic, while it is isotropic and randomly far away from the grain boundary. For grain boundaries with lower atom mobility constant, the curvature driven grain boundary migration process and the spinodal decomposition process happen simultaneously, and the beta phase is concentric ring-like and parallel to the grain boundary. For grain boundaries with higher atom mobility constant, the spinodal decomposition velocity is increased either, now the spinodal patterns tend to be perpendicular to the original grain boundaries. The simulation results of 2D and 3D are consistent. Further, we investigated the influence of

grain boundary energy and concentration gradient energy on the spinodal decomposition process. With the increase of concentration gradient energy, the spinodal decomposition velocity decreases gradually and the influence of the moving grain boundary on the spinodal decomposition becomes weaker. The influence of grain boundary energy on the spinodal decomposition process is a bit complicated, as the increase of k_η the morphology of the grain boundary modulated beta phase shifts from layer-shaped to flake-shaped, similar results have been reported by Yang et al. [33] and Deng et al. [7].

CRediT authorship contribution statement

Guo Can: Conceptualization, Investigation, Funding acquisition, Supervision, Writing – original draft. **Gao Ying:** Investigation, Data curation, Writing – original draft. **Cui Yu-teng:** Software, Methodology. **Zhao Yu-ping:** Visualization, Investigation. **Xu Chun-jie:** Conceptualization, Writing – review & editing. **Sui Shang:** Formal analysis. **Wu Xiang-quan:** Validation. **Zhang Zhong-ming:** Resources, Writing – review & editing.

Declaration of Competing Interest

The authors declare that they have no known competing financial interests or personal relationships that could have appeared to influence the work reported in this paper.

Data availability

No data was used for the research described in the article.

Acknowledgements

This work was supported by the Natural Science Foundation of Shaanxi Province (2023-JC-QN-0573, 2023-GHZD-50), the National Natural Science Foundation of China (51801154), the Science and Technology Plan Project of Xi'an (2022JH-RYFW-0026).

References

- [1] T. Meiners, T. Frolov, R.E. Rudd, G. Dehm, C.H. Liebscher, Observations of grain-boundary phase transformations in an elemental metal, *Nature* 579 (2020) 375–378.
- [2] F. Cao, Y. Chen, S. Zhao, E. Ma, L. Dai, Grain boundary phase transformation in a CrCoNi complex concentrated alloy, *Acta Mater.* 209 (2021) 116786.
- [3] T.G. Lach, W.E. Frazier, J. Wang, A. Devaraj, T.S. Byun, Precipitation-site competition in duplex stainless steels: Cu clusters vs spinodal decomposition interfaces as nucleation sites during thermal aging, *Acta Mater.* (2020).
- [4] S. Rajeshwari K, S. Sankaran, K.C. Hari Kumar, H. Rösner, M. Peterlechner, V. A. Esin, S. Divinski, G. Wilde, Grain boundary diffusion and grain boundary structures of a Ni-Cr-Fe- alloy: Evidences for grain boundary phase transitions, *Acta Mater.* 195 (2020) 501–518.
- [5] A. Kwiatkowski da Silva, R.D. Kamachali, D. Ponge, B. Gault, J. Neugebauer, D. Raabe, Thermodynamics of grain boundary segregation, interfacial spinodal and their relevance for nucleation during solid-solid phase transitions, *Acta Mater.* 168 (2019) 109–120.
- [6] L. Li, Z. Li, A. Kwiatkowski da Silva, Z. Peng, H. Zhao, B. Gault, D. Raabe, Segregation-driven grain boundary spinodal decomposition as a pathway for phase nucleation in a high-entropy alloy, *Acta Mater.* 178 (2019) 1–9.
- [7] Y.-Y. Deng, C. Guo, J.-C. Wang, Q. Liu, Y.-P. Zhao, Q. Yang, Phase-field study of spinodal decomposition under effect of grain boundary*, *Chin. Phys. B* 30 (2021), 088101.
- [8] K. Grönhagen, J. Ågren, M. Odén, Phase-field modelling of spinodal decomposition in TiAlN including the effect of metal vacancies, *Scr. Mater.* 95 (2015) 42–45.
- [9] J. Liu, X. Wu, W.N. Lennard, D. Landheer, M.W.C. Dhama-Wardana, Surface-directed spinodal decomposition in the pseudobinary alloy $HfO_2x(SiO_2)_{1-x}$, *J. Appl. Phys.* 107 (2010), 123510.
- [10] Y. Li, H. Katsui, T. Goto, Microstructure evolution of (Ti, Zr)C solid solution at the initial stage of phase decomposition, *Mater. Today Proc.* 4 (2017) 11449–11452.
- [11] Y.-S. Li, S.-X. Li, T.-Y. Zhang, Effect of dislocations on spinodal decomposition in Fe-Cr alloys, *J. Nucl. Mater.* 395 (2009) 120–130.
- [12] E.R. Homer, O.K. Johnson, D. Britton, J.E. Patterson, E.T. Sevy, G.B. Thompson, A classical equation that accounts for observations of non-Arrhenius and cryogenic grain boundary migration, *npj Comput. Mater.* 8 (2022) 157.

- [13] X. Lu, C. Dong, X. Guo, J. Ren, H. Xue, F. Tang, Y. Ding, Effects of grain size and temperature on mechanical properties of nano-polycrystalline Nickel-cobalt alloy, *J. Mater. Res. Technol.* 9 (2020) 13161–13173.
- [14] X. Zhou, R. Darvishi Kamachali, B.L. Boyce, B.G. Clark, D. Raabe, G.B. Thompson, Spinodal decomposition in nanocrystalline alloys, *Acta Mater.* 215 (2021), 117054.
- [15] J.M. Monti, E.M. Hopkins, K. Hattar, F. Abdeljawad, B.L. Boyce, R. Dingreville, Stability of immiscible nanocrystalline alloys in compositional and thermal fields, *Acta Mater.* 226 (2022), 117620.
- [16] S.Y. Hu, L.Q. Chen, Spinodal decomposition in a film with periodically distributed interfacial dislocations, *Acta Mater.* 52 (2004) 3069–3074.
- [17] D.J. Seol, S.Y. Hu, Y.L. Li, J. Shen, K.H. Oh, L.Q. Chen, Computer simulation of spinodal decomposition in constrained films, *Acta Mater.* 51 (2003) 5173–5185.
- [18] M.L. Steyn-Ross, D.A. Steyn-Ross, L.J. Voss, J.W. Sleigh, Spinodal decomposition in a mean-field model of the cortex: emergence of hexagonally symmetric activation patterns, *Phys. Rev. E* 99 (2019), 012318.
- [19] J. Lee, K. Chang, Effect of magnetic ordering on the spinodal decomposition of the Fe-Cr system: a GPU-accelerated phase-field study, *Comp. Mater. Sci.* 169 (2019), 109088.
- [20] R. Chafle, S. Bhowmick, R. Mukherjee, Domain boundary assisted spinodal decomposition in magnetic materials, *Mater. Lett.* 324 (2022), 132630.
- [21] J. Zhang, J. Su, B. Zhang, Y. Zong, Z. Yang, C. Zhang, H. Chen, Phase-Field Modeling of Hydrogen Diffusion and Trapping in Steels, *Acta Metall. Sin. (Engl. Lett.)* (2021) 1–6.
- [22] S. Zhang, W. Jiang, M.R. Tonks, A new phase field fracture model for brittle materials that accounts for elastic anisotropy, *Comput. Method. Appl. Methods* 358 (2020), 112643.
- [23] M.-T.W. Yu-Hao Song, Jia Ni, Jian-Feng Jin, Y.-P. Zong, Effect of grain boundary energy anisotropy on grain growth in ZK60 alloy using a 3D phase-field modeling, *Chin. Phys. B* 29 (2020), 128201.
- [24] T. Zhang, D. Wang, Y. Wang, Novel transformation pathway and heterogeneous precipitate microstructure in Ti-alloys, *Acta Mater.* 196 (2020) 409–417.
- [25] Y.H. Wang, D.C. Zhang, Z.P. Pi, J.G. Lin, C. Wen, Phase field simulation of spinodal decomposition in Zr-Nb alloys for implant materials, *J. Appl. Phys.* 126 (2019), 085102.
- [26] R. Chafle, S. Bhowmick, R. Mukherjee, Effect of co-existing external fields on a binary spinodal system: a phase-field study, *J. Phys. Chem. Solids* 132 (2019) 236–243.
- [27] H. Ramanarayanan, T.A. Abinandanan, Grain boundary effects on spinodal decomposition: II. Discontinuous microstructures, *Acta Mater.* 52 (2004) 921–930.
- [28] C. Guo, J. Wang, Z. Wang, J. Li, Y. Guo, Y. Huang, Interfacial free energy adjustable phase field crystal model for homogeneous nucleation, *Soft Matter* 12 (2016) 4666–4673.
- [29] H. Ramanarayanan, T.A. Abinandanan, Phase field study of grain boundary effects on spinodal decomposition, *Acta Mater.* 51 (2003) 4761–4772.
- [30] M.R. Tonks, D. Gaston, P.C. Millett, D. Andrs, P. Talbot, An object-oriented finite element framework for multiphysics phase field simulations, *Comp. Mater. Sci.* 51 (2012) 20–29.
- [31] Y. Ishiguro, Y. Tsukada, T. Koyama, Phase-field simulation of spinodal decomposition and its effect on stress-induced martensitic transformation in Ti-Nb-O alloys, *Comp. Mater. Sci.* 151 (2018) 222–230.
- [32] S. Sugathan, S. Bhattacharya, A phase-field study of elastic stress effects on phase separation in ternary alloys, *Comp. Mater. Sci.* 172 (2020), 109284.
- [33] T. Yang, Z. Chen, J. Zhang, W.-P. Dong, L. Wu, Effect of grain boundary on spinodal decomposition using the phase field crystal method, *Chin. Phys. Lett.* 29 (2012) 1–4.